Phase Transitions in Emulsified HNO_3/H_2O and $HNO_3/H_2SO_4/H_2O$ Solutions

Hung-Yau A. Chang,† Thomas Koop, Luisa T. Molina, and Mario J. Molina*

Department of Earth, Atmospheric, and Planetary Sciences and Department of Chemistry, Massachusetts Institute of Technology, Cambridge, Massachusetts 02139

Received: October 21, 1998; In Final Form: January 26, 1999

The liquid−solid phase transitions of emulsified binary HNO_3/H_2O and ternary $HNO_3/H_2SO_4/H_2O$ acid solutions have been investigated using differential scanning calorimetry in order to elucidate the mechanism of ice formation from stratospheric aerosols. The results indicate that binary solution droplets with less than 33 wt % HNO_3 freeze to form ice at temperatures 37−65 K below the equilibrium ice melting temperatures. Droplets with higher concentrations (up to 65 wt %) do not freeze; instead, they form glasses at temperatures below 160 K. The results also show that the presence of H_2SO_4 in amounts corresponding to less than 5 wt % depresses the freezing points of the 0−33 wt % HNO_3 droplets by 5 to >30 K, in agreement with earlier observations. The implications of the new data for our understanding of the formation of polar stratospheric clouds have been investigated using a thermodynamic model. The results indicate that an ice saturation ratio of greater than 1.65 is required for ice particles to form from ternary aerosols at stratospheric temperatures, corresponding to a cooling of about 3 K below the ice frost point.

1. Introduction

It is now well established that heterogeneous chemical reactions on surfaces of stratospheric sulfate aerosols (SSAs) and polar stratospheric clouds (PSCs) in the lower stratosphere are responsible for the catalytic destruction of polar ozone through the release of reactive chlorine species from their nonreactive reservoir forms.[1−3] It is therefore important to know the chemical composition and physical state of these particles in order to estimate the appropriate rates of the heterogeneous reactions. Of particular interest are the conditions under which liquid−solid transformations occur. To date, the process that has received the most attention is the formation of nitric acid trihydrate (NAT) particles (type Ia PSCs) from the background sulfate aerosols during the polar winter.[4−7]

Despite numerous experimental and modeling efforts, the formation mechanisms of solid PSCs at temperatures above the ice frost point remain controversial. Evidence for the existence of another kind of PSCs particles (type Ib), which consist of liquid aerosols, has shifted most of the attention to the unusually strong supercooling potential of ternary $H_2SO_4/HNO_3/H_2O$ acid mixtures.[4,8,9] Studies of the liquid−solid transition of this ternary mixture using bulk size samples have produced inconsistent results[9,10] because of the existence of unavoidable heterogeneous surfaces (e.g., suspended dust particles and container wall surface). However, it is now generally agreed that these ternary aerosols do not freeze above the ice frost point;[9] therefore, it is of importance to understand under which conditions ice will freeze from these mixtures. In this study we make use of emulsified samples, i.e., micrometer-sized droplets in an inert oil matrix, to study the nucleation of ice from stratospherically relevant HNO_3/H_2O and $HNO_3/H_2SO_4/H_2O$ solutions.

The use of emulsions for the investigation of homogeneous nucleation was first proposed by Vonnegut[11] in the late 1940s. Since then, this technique has been used for the study of supercooling properties of a wide variety of materials such as water,[12,13] lithium chloride,[14] gallium[15] or tellurium-x copper alloys,[16] and acid solutions.[17] This technique also makes it possible to vitrify molecular liquids, which were not previously thought to be glass-forming.[18] In general, the material under investigation is dispersed in stable micrometer-sized droplets in a medium containing an emulsifier. The medium is usually chosen in such a way that it freezes or vitrifies at a temperature much lower than the expected maximum supercooling of the dispersed phase. Also, the emulsifier should be strongly adsorbed at the droplet/medium interface while having negligible solubility in the droplet phase. This turns out to be a crucial requirement, as the presence of emulsifier in the dispersed aqueous phase could significantly alter its physical properties and hence the phase transition temperature. In this study, halocarbon oil is selected as the hydrophobic medium for its inertness to acid and oxidizing agents, while lanolin, a proven effective emulsifier for water, is used to decrease the surface tension between the acid and the halocarbon oil.

2. Experimental Section

2.1. Differential Scanning Calorimetry. Differential scanning calorimetry (DSC) has been widely used for the characterization of both isothermal and nonisothermal crystallization behaviors. The unique feature of this particular technique is that the temperature scan rate can be controlled with extremely high accuracy. If the size of the sample is small enough and good thermal contact is maintained with the sample pan throughout the experiment, the thermal behavior of the system can be used to accurately determine the phase transformation characteristics of the sample.

The experimental setup employed in this paper has been described in detail elsewhere.[19] A Perkin-Elmer DSC-7 is used

* To whom correspondence should be addressed.
† Current address: Hong Kong Government Environmental Protection Department, 33/F., Revenue Tower, 5 Gloucester Road, Wan Chai, Hong Kong.

10.1021/jp9841034 CCC: $18.00 © 1999 American Chemical Society
Published on Web 03/25/1999

in this study; it operates on the power-compensated null-balance principle (temperature precision of ±0.1 K) to ensure that both the sample and the reference cells have the same predetermined rate of temperature change. In general, the technique involves monitoring the difference between the electric power supplied to heat the sample cell and the reference cell so that the temperature difference between the cells is always maintained close to zero. The maximum sensitivity of the DSC-7 is around 0.1 mcal s^{-1} for a full-scale deflection. Normally, only a few milligrams of sample are required for each measurement. The operational temperature ranges from 100 to 450 K. The cell temperature was calibrated using a Perkin-Elmer two-point calibration program with *n*-dodecane (Fisher Scientific, Purified Grade, mp 263.50 K) and cyclohexane GR (EM Science, solid−solid transition at 186.09 K) as the standards. This calibration is used for both cooling and heating experiments. Recent studies[20,21] using high-purity liquid crystals such as 99.9% (+)-4-*n*-hexyloxyphenyl-4′-(2′-methylbutyl)biphenyl 4-carboxylate and *N*-(4-*n*-octyloxy-2-hydroxybenzal)-4′-*n*-butylaniline, which have no tendency to supercool, have shown that if the heating or cooling rate does not exceed 20 K/min, the standard deviation of the accuracy of the measured transition temperatures during cooling is only about ±0.3 K. In this study, moderate scanning rates of 3 and 1 K/min were chosen for the heating and cooling measurements, respectively. The eutectic and melting temperatures of the emulsion samples are practically the same as those obtained using bulk nitric acid solutions.

Indium (99.99%, $\Delta H_{\text{Fusion}} = 28.48$ J/g, mp 429.75 K) was selected as the calibration standard for the heat of transition mainly because of its excellent reproducibility and well-established value of ΔH. The maximum deviation of ΔH measured using the DSC-7 was found to be less than 0.1%. Both the sample and reference cell compartments were purged with helium during the experiment to prevent any unwanted condensation at low temperatures. A closed platinum capsule pan designed for volatile samples was used. It has the distinct advantage of retaining practically all the sample throughout the experiment; the maximum weight loss was found to be less than 1%.

2.2. Sample Preparation and Stability. Bulk acid mixtures were prepared by diluting 95.6 wt % sulfuric acid and 67 wt % nitric acid (Mallinckrodt, Analytical Grade) with the appropriate amount of deionized water. The accuracy of this method was estimated to be around ±0.1 wt %. The emulsion samples used in this study were made by mixing the acid solutions with an oil phase containing approximately 80 wt % halocarbon oil series 0.8 (Halocarbon Products Corporation) and 20 wt % lanolin (Aldrich Chemical). Halocarbon oil series 0.8 is a blend of completely halogenated chlorofluoroethylene oils and is inert to practically all acids, alkalis, and oxidizing agents. The weight fraction of the dispersed acid phase in the emulsions was ~0.1 for all samples. Emulsification was carried out by shaking the volumetric flasks containing the acid-in-oil mixtures (A/O) at room temperature for about 1 min, first manually and then with a high-speed mixer (Thermolyne Maxi-Mix III, type 65800). This procedure was repeated for every new sample loaded into the DSC. Approximately 20 ± 3 μL of the emulsion sample were used for each measurement.

The glass transition temperature (T_g) of the halocarbon oil/lanolin mixture was determined to be around 123 K. For the acids T_g is generally in the range from 140 to 160 K; hence, appreciable changes in the oil/lanolin system owing to its glass transition can occur only 20 K or more below the glass points of the aqueous phase.

Lanolin is a natural compound extracted from sheep wool and consists mostly of a complex mixture of esters, and hence, its stability in concentrated acids is not well characterized. However, our control experiments indicate that there is no appreciable reaction between the acid samples and the halocarbon oil or the lanolin emulsifier. Lanolin did not appear to be soluble in the nitric acid solution nor did it show any type of chemical reaction. This is corroborated by the fact that the heating thermograms for two 52.8 wt % nitric acid samples, one without lanolin and the other an hour after adding lanolin, were essentially identical. For the sample containing the lanolin, further heating thermograms were taken 2 days and 1 month after sample preparation. The thermogram for the 2-day-old sample was essentially the same as the one for the freshly prepared sample. Not only were the transition temperatures the same for both thermograms but the area ratio of the eutectic peak to the melting peak remained the same as well. Only the 1-month-old sample revealed a slightly lower melting point, implying that either a very slow reaction occurred between the acid and the lanolin or the evaporation of water may have slightly changed the composition of the nitric acid solution.

The same method was used to test the stability of lanolin in sulfuric acid solutions (5 and 10 wt %); DSC measurements were performed 6 days after the preparation of the samples. The emulsion with lanolin remained clear even 2 weeks after the measurement. We found that there is essentially no difference between the transition peaks for the samples with and without lanolin. For the cases of extremely concentrated acid only (e.g., 77−83 wt % H_2SO_4), the emulsion developed into a dark-brown color almost instantaneously. The sudden change in color is most likely attributable to the dehydration of lanolin. To prevent any degradation of the lanolin, all the DSC experiments described below were performed within 4 h after the preparation of the samples.

Other emulsion systems using fluorosurfactants (DuPont, Zonyl FSN-100 and FSO-100) instead of lanolin were tested initially, as it appeared that the excellent chemical inertness of the fluorosurfactants would be ideal for our purpose. Unfortunately, we soon found that the solubility of these surfactants in aqueous solutions is relatively high (≥0.1 g of solid/100 g of solution), and hence, quaternary instead of ternary systems were obtained. The DSC thermograms for these emulsions indicate that the freezing temperature depends strongly on the amount of fluorosurfactant in the emulsions. For instance, the freezing temperature for a 52.8 wt % HNO_3/H_2O emulsion decreases from 215 to 193 K when the weight fraction of the fluorosurfactant FSN-100 increases from 0.095 to 0.915. Moreover, the equilibrium melting point of this system shifts slightly to the lower temperature side, indicating an enhanced solute effect of the fluorosurfactants.

2.3. Analysis of the Data. The extent of crystallization (ξ), defined as the weight fraction of the crystallized phase, can be accurately estimated by integrating directly the DSC exothermic peak obtained during a temperature scan. The sensitivity of the signals (i.e., the area under the peaks) is directly proportional to the temperature scan rate. The entire transition process lasts typically 6−7 min. Figure 1 shows the DSC thermogram of a ternary acid emulsion sample with 5 wt % HNO_3 and 1 wt % H_2SO_4 taken at a constant cooling scan rate of 1 K/min. The onset temperature T_i (time $t = 0$), chosen arbitrarily in this case, is defined as the temperature above which no crystallization events are detected. The deviation of the curve from the baseline at some particular temperature T at time $t = t'$ is simply a measure of the heat flow from the sample, i.e., dH/dt, where H

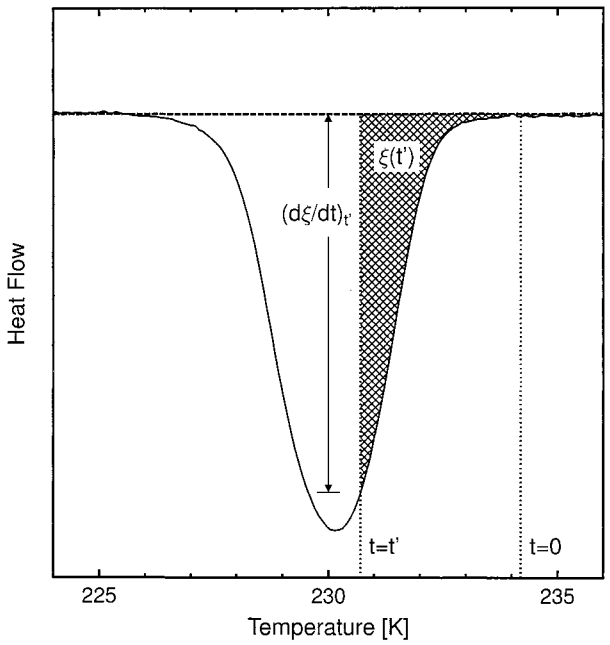

Figure 1. DSC thermogram of a ternary acid emulsion containing 5 wt % HNO_3 and 1 wt % H_2SO_4, recorded with a cooling rate of 1 K/min.

is the sample enthalpy. As a first approximation, one can apply the Borchard assumption[22, 23]

$$\frac{dH}{dt} \propto \frac{d\xi}{dt}$$

and hence, the area above the curve and under the baseline between time $t = 0$ to $t = t'$ (the shaded region in Figure 1) is roughly proportional to $\xi(t')$. The proportionality constant can be readily determined from the normalization condition

$$\int_0^\infty \frac{d\xi}{dt}\,dt = 1$$

In general, all emulsion samples studied here exhibit the same crystallization curve depicted in Figure 1.

Temperature scan rates in the experiments described below were chosen to be 1 K/min. This was done with the consideration of two particular requirements in mind. On one hand, a slower scan rate ensures that the sample is always in thermal equilibrium with the thermostated sample holder; i.e., there is no thermal lag between the recorded temperature and the actual sample temperature. On the other hand, faster scan rates yield higher signal-to-noise ratios. Figure 2 shows a compilation of thermograms for an emulsion sample at varying cooling rates.

The experiments shown in Figure 2 were repeated for different solution compositions, and the resulting freezing points are plotted in Figure 3 as a function of the inverse cooling rate. As can be seen from Figure 3, a cooling rate of 1 K/min has a negligible effect on the freezing point while revealing a good signal-to-noise ratio. Hence, in all the experiments discussed below a cooling rate of 1 K/min was used.

3. Results and Discussion

3.1. Droplet Size Distribution. One of the main advantages of studying phase transitions using the acid/oil emulsion system is that all the aqueous droplets are isolated by the oil phase, and hence, there is essentially no molecular exchange between

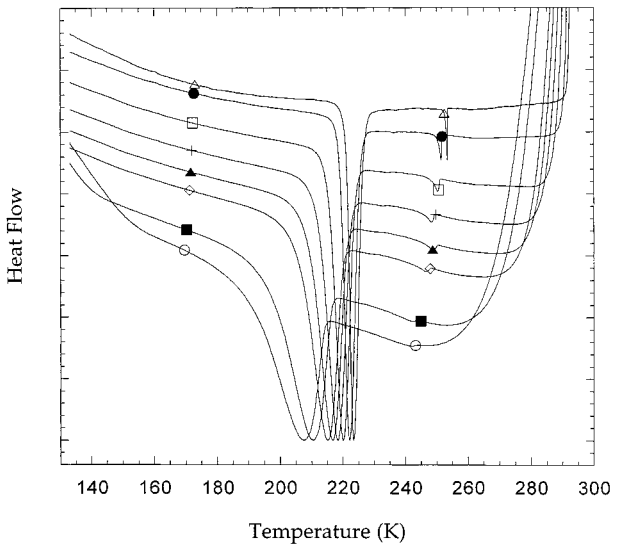

Figure 2. DSC thermograms of a ternary acid emulsion containing 5 wt % HNO_3 and 5 wt % H_2SO_4, recorded with varying cooling rates of 5 (upper curve with open triangles), 10, 20, 30, 40, 50, 80, and 100 K/min (lower curve with open circles).

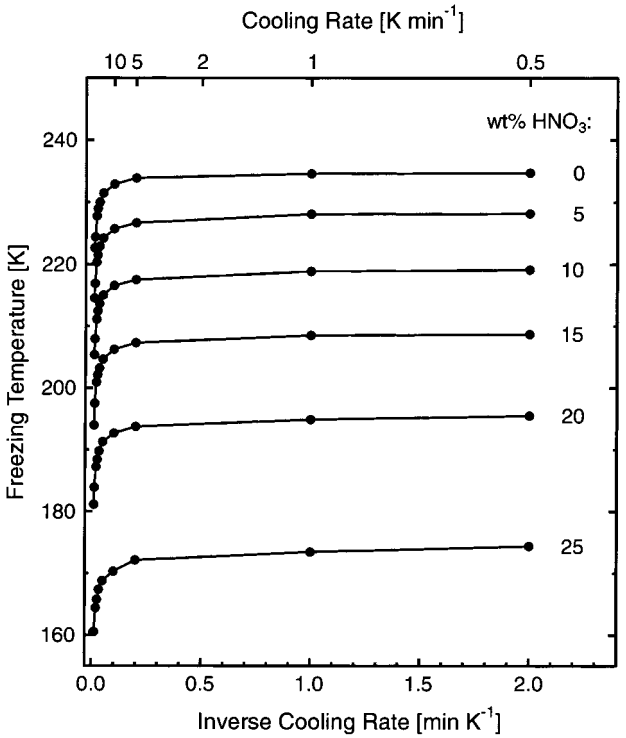

Figure 3. Dependence of the freezing temperature on the inverse cooling rate for ternary emulsions containing 5 wt % H_2SO_4 and 0−25 wt % HNO_3. The numbers on the right indicate the HNO_3 concentration for each data set.

the droplets during the cooling and warming processes. This ensures that the composition of the microdroplets remains the same throughout the experiment. Furthermore, the results obtained in this way already have a statistical meaning because of the fact that a large number of aqueous droplets ($\sim 10^6$) are involved in each DSC measurement. The morphology of the emulsified aqueous droplets at sub-zero temperatures was studied using a transmission optical microscope equipped with a cooling stage. Although most of the droplets appear to be roughly spherical, some of them (especially the smaller ones) are irregular in shape. The reason for this is not clear; it may be related to the relatively high concentration of lanolin in the

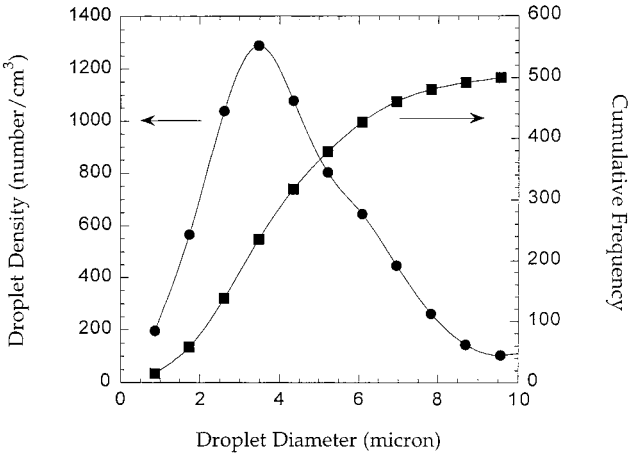

Figure 4. Droplet size distribution and cumulative frequency for a 1 wt % HNO_3 emulsion. The weight fraction of the aqueous phase is 0.1, and the total number of droplets is 510.

oil phase. The average distance between the centers of the droplets is estimated to be around 8 μm.

Since the nucleation probability is proportional to the volume, knowledge of the size distribution of the emulsion droplets becomes important. Seven photographs taken with the optical microscope were analyzed for the droplet size distribution of the 1 wt % HNO_3/H_2O acid emulsion. In order not to underestimate the average droplet size, the largest dimension of an irregular droplet was chosen as the diameter. The resulting droplet size distribution is shown in Figure 4. Droplets with a diameter larger than 10 μm are very rare in the acid emulsions and are not represented in the figure. The average radius of the 510 droplets evaluated was found to be approximately 2.3 μm.

3.2. Freezing Points. *3.2.1. HNO_3/H_2O Solutions.* Emulsified samples of binary HNO_3/H_2O solutions have been investigated in the concentration range from 0 to 65 wt % HNO_3. Parts a and b of Figure 5 show cooling and heating thermograms of such solutions with concentrations smaller than 33 wt % HNO_3. During cooling, freezing of ice was observed for the composition range 0−32.5 wt % HNO_3. Crystallization upon heating was detected for the 35, 63.6, and 65 wt % nitric acid emulsions, while for the 40.3 wt % case, freezing upon cooling to NAT and ice was observed only in some samples. In addition, the glass transition (T_g) was observed during warming through the typical jump in heat capacity associated with the onset of fast molecular diffusion above the glass point for all samples that did not crystallize upon cooling, with an uncertainty of ±2 K.

Figure 6 depicts a summary of the freezing points measured for the binary HNO_3/H_2O system. The freezing points of the emulsions were determined as the temperature where 90% of the sample mass was frozen, i.e., $\xi = 0.9$. This corresponds to the freezing temperature for a droplet size of 2.5 μm. Also, the observed glass transition temperatures are shown for the more concentrated solutions. As can be seen in the figure, T_g increases linearly with the weight percentage of nitric acid. The experimentally observed T_g values are in good agreement with published values on the HNO_3/H_2O system.[17,24] By extrapolating the freezing temperature (T_f) to lower temperatures and T_g to lower concentrations, we determine the HNO_3 concentration for which $T_f = T_g$ to be ∼39 wt %; hence, ice freezing during cooling cannot occur for compositions greater than 39 wt %. Note that this concentration is slightly larger than the eutectic concentration (33.5 wt %) of NAT/ice.

Figure 7 shows the degree of supercooling as a function of the melting (T_m) and freezing (T_f) temperatures for the binary

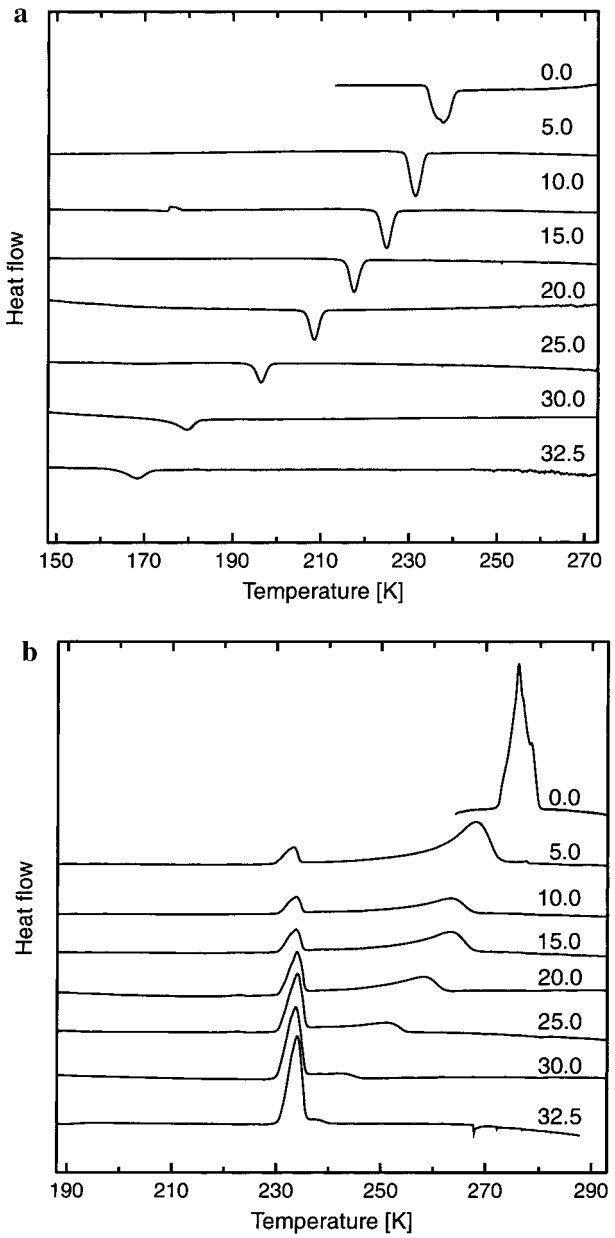

Figure 5. DSC thermograms for binary HNO_3/H_2O solutions 0−32.5 wt % in composition: (a) cooling runs; (b) heating runs.

HNO_3/H_2O emulsion system. We found that both sets of data can be approximated by a linear relationship, with the supercooling changing more rapidly with T_m than T_f. This is in disagreement with the conclusions of Hallett and Lewis,[25] who suggested that in general the maximum supercooling for ice-forming solution droplets would be the same as the maximum supercooling of pure water droplets (∼40 K). As can be seen in the figure, Hallett and Lewis' hypothesis does not apply to the case of binary nitric acid emulsions with acid concentrations ranging from 0 to 32.5 wt %. Instead, the equation

$$T_f[K] = 1.645T_m[K] - 214.15$$

is found to be more appropriate. The homogeneous nucleation temperature (T^*) for a wide variety of glass-forming materials has been measured, and the results indicate that T^* for nearly all materials studied lies between $0.75T_m$ and $0.85T_m$.[26] In the binary nitric acid emulsion system studied here T* varies from $0.86T_m$ for pure H_2O to $0.72T_m$ for 32.5 wt % HNO_3.

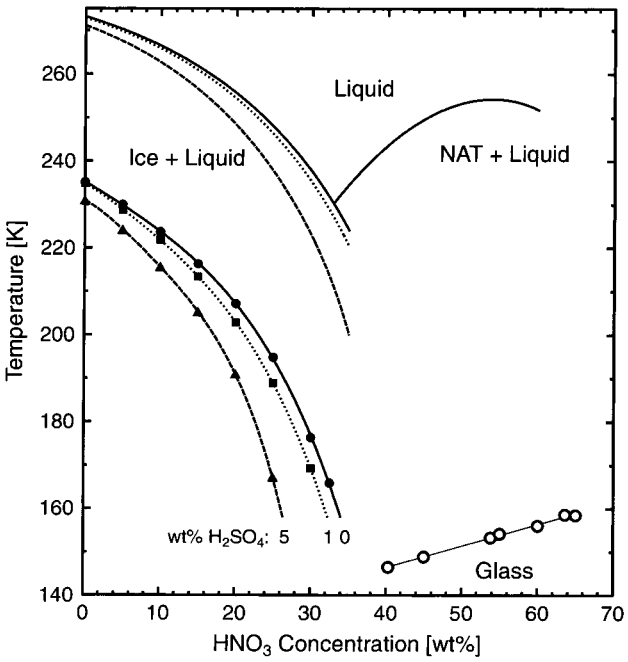

Figure 6. Freezing points of binary and ternary solutions to form ice as a function of HNO_3 concentration for 0, 1, and 5 wt % H_2SO_4 (indicated by the solid circles, squares, and triangles, respectively). Melting points of ice and NAT are also shown for the binary HNO_3/H_2O system as solid lines. The ice melting point curves for ternary solutions containing 1 and 5 wt % H_2SO_4 are shown for comparison as dotted and dashed lines without symbols, respectively. The glass points are indicated as open circles.

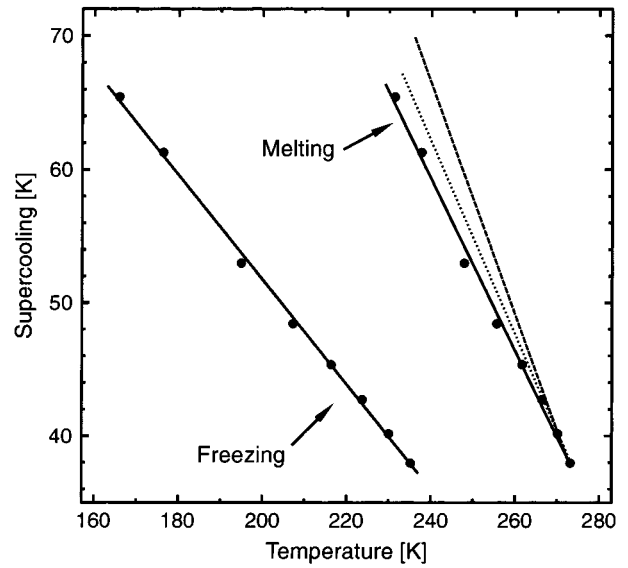

Figure 7. Supercooling as a function of freezing and melting temperatures for the binary HNO_3/H_2O emulsion system (circles and solid lines). The freezing points are the experimentally determined values while the melting points have been taken from the thermodynamic model of Carslaw et al.[37] For comparison, the supercooling as a function of the ice melting temperature is also shown for the ternary solutions containing 1 and 5 wt % H_2SO_4 (dotted and dashed lines, respectively).

As mentioned above, we did not observe freezing upon cooling of either NAT or NAD from their stoichiometric solutions (53.8 and 63.6 wt % HNO_3, respectively). This is in disagreement with earlier aerosol measurements with a settling chamber or with flow tube experiments.[27−31] In these experiments NAT and NAD formed at temperatures between about 163 and 180 K[30,31] or between 189 and 204 K.[27−29] The nucleation rate coefficients of 10^7-10^{12} cm^{-3} s^{-1} that were observed in these experiments should be large enough to induce freezing in our experiments. However, at present we have no explanation neither for the fact that freezing is observed in these aerosol measurements and not in our experiments nor for the differences in freezing temperature between the settling chamber and flow tube experiments.

3.2.2. $HNO_3/H_2SO_4/H_2O$ Solutions. Sulfuric acid is known to have a higher tendency to supercool than nitric acid, and recent experiments in our laboratory have further corroborated this finding.[32] The effect of sulfuric acid on the supercooling properties of emulsified nitric acid solutions is also of interest. Recent results from the freezing experiments of Koop et al.[33] and Meilinger et al.[34] on ternary $H_2SO_4/HNO_3/H_2O$ bulk solutions have shown that even very small amounts of sulfuric acid (e.g., $\leq$2.5 wt %) can hinder the nucleation of NAT in the ternary acid system. To investigate this effect for the case for micrometer-sized droplets, we studied emulsified ternary acid solutions containing 1 and 5 wt % of H_2SO_4. For the solutions containing 1 wt % of H_2SO_4, all samples except the one with 35 wt % HNO_3 show an exothermic (freezing) peak during the cooling process. The area under the exothermic peaks decreases as the acid concentration increases, implying the formation of ice as the main phase transformation process during cooling. Only the binary ice/NAT eutectic and the ice melting peaks are observed in the heating thermograms. The ternary eutectic peaks are probably too small to be observable. DSC thermograms were also recorded for ternary acid emulsion samples with 5 wt % H_2SO_4 and 0−35 wt % HNO_3. Unlike the 1 wt % H_2SO_4 emulsion samples described in the previous paragraph, the ternary eutectic transition peak can be clearly observed for many samples, especially those with a higher concentration of nitric acid.

The ice freezing points for the ternary emulsion system are also plotted in Figure 6 as squares (1 wt % H_2SO_4) and triangles (5 wt % H_2SO_4). As can be seen in the figure, the ice freezing points of the ternary solutions are lower than the binary ones (circles) by up to 25 K. However, this is mainly due to the fact that the equilibrium ice melting points are also reduced by the presence of H_2SO_4, as indicated by the lines without symbols (dotted line, 1 wt % H_2SO_4; dashed line, 5 wt % H_2SO_4). Thus, taking into account this effect, the actual increase in supercooling is only a few degrees Kelvin. This increase is shown more explicitly in Figure 7; the solid line labeled "Melting" represents the supercooling as a function of the equilibrium ice melting temperature for the binary HNO_3/H_2O solutions. In addition, the supercooling for the ternary solutions containing 1 wt % H_2SO_4 (dotted line) and 5 wt % H_2SO_4 (dashed line) is shown in Figure 7 as well.

We can use Figure 7 to compare the degree of supercooling for different solutions having the same melting temperature—and consequently, the same water activity. It is clear that the solution containing the most H_2SO_4 requires the highest supercooling for the formation of ice, e.g., a supercooling of 66.4 K for the 5 wt % H_2SO_4 solution, which has an ice melting temperature of 240 K, in comparison to a supercooling of 59.3 K for the binary HNO_3/H_2O solution, which has the same melting point. An even better approach is to compare the water activity of the different solutions at the freezing point rather than their weight fraction. This will be explained in the following section.

4. Atmospheric Implications

The ice freezing points described above can be used to determine whether binary and ternary acid aerosols are likely

TABLE 1: Parametrizations for the Critical Freezing Temperature (T_f) as a Function of HNO_3 Composition and for the Critical Saturation Ratio (S_{Ice}*) and the Cooling below the Ice Frost Point (ΔT*) as a Function of Temperature[a]

Y*	X	H_2SO_4 [wt %]	A_0	A_1	A_2	A_3	A_4	range of validity
T_f	HNO_3 [wt %]	0	235.23	−1.0234	-1.054×10^{-2}	0.068×10^{-3}	-0.247×10^{-4}	0−32.5 wt %
T_f	HNO_3 [wt %]	1	234.92	−1.1037	-2.509×10^{-2}	0.764×10^{-3}	-0.377×10^{-4}	0−30 wt %
T_f	HNO_3 [wt %]	5	231.00	−0.9845	-9.754×10^{-2}	6.091×10^{-3}	-1.88×10^{-4}	0−25 wt %
S_{ice}*	T	0	1.294	0.7222×10^{-2}	-2.802×10^{-5}			185−235 K
S_{ice}*	T	1	0.851	1.2095×10^{-2}	-4.083×10^{-5}			185−235 K
S_{ice}*	T	5	0.897	1.1581×10^{-2}	-3.940×10^{-5}			185−231 K
ΔT*	T	0	−4.63	0.1005	-0.819×10^{-3}	1.7645×10^{-6}		185−235 K
ΔT*	T	1	−9.25	0.1807	-1.281×10^{-3}	2.6351×10^{-6}		185−235 K
ΔT*	T	5	−28.78	0.4640	-2.644×10^{-3}	4.8101×10^{-6}		185−231 K

[a] The different critical parameters, Y*, are a function of X and can be calculated from $Y^* = \sum_{i=0}^{4} A_i X^i$. The ranges over which these parametrizations are valid are given in the last column.

to freeze in the lower winter polar stratosphere. To accomplish this, we performed some thermodynamic calculations to relate our freezing results to the atmosphere. We also compare our results to data obtained from a model developed recently by Tabazadeh et al.,[35] which they used to predict the conditions under which ice particles (type II polar stratospheric clouds) would nucleate from stratospheric aerosols in the lower stratosphere. Since no laboratory measurements were available for the HNO_3/H_2O system, these authors utilized instead the freezing properties of the H_2SO_4/H_2O system.

In the following we discuss how incorporating the new ice freezing point data shown in Figure 6 affects the critical parameters for the formation of ice particles from HNO_3 aerosols and also what effect small amounts of H_2SO_4 have on their freezing properties. The water saturation vapor pressure and the ice saturation vapor pressure were taken from Tabazadeh et al.,[36] and the water activity in the liquid phase was calculated from the model of Carslaw et al.[37] The critical HNO_3 concentration and the critical temperature for ice nucleation determined experimentally were used as input data (see Figure 6). The two most important parameters in terms of cloud modeling and observations are probably the critical saturation ratio with respect to ice, S_{ice}*, and the critical cooling below the ice frost point, ΔT*, needed to form the ice particles. S_{ice}* was calculated as

$$S_{ice}^* = P_{H2O}^*(T^*,\mathrm{wt}^*)/P_{ice}(T^*)$$

where P_{H2O}*(T*,wt*) is the equilibrium water partial pressure of an HNO_3/H_2O or $HNO_3/H_2SO_4/H_2O$ aerosol at the critical temperature T* and the critical composition wt*, and P_{ice} (T*) is the water vapor pressure of ice at T*. The critical cooling below the ice frost point, ΔT*, was calculated from

$$\Delta T^* = T_{ice}(P_{H2O}^*) - T^*$$

where $T_{ice}(P_{H2O}$*) is the atmospheric ice frost point temperature for the critical water partial pressure P_{H2O}* at T*.

Both S_{ice}* and ΔT* are plotted as a function of temperature in Figure 8. The solid lines indicate S_{ice}* and ΔT* for binary HNO_3/H_2O aerosols based on our experimental results and the dotted and dashed lines for ternary $HNO_3/H_2SO_4/H_2O$ aerosols containing 1 and 5 wt % of H_2SO_4, respectively. Finally, the dash−dotted lines indicate the results Tabazadeh et al.[29] derived for binary HNO_3/H_2O aerosols. Note that this parametrization is for aerosols with a diameter of 0.2 μm while our parametrization is derived for 2.5 μm aerosols, as determined experimentally. The parametrization of Tabazadeh et al.[35] shows a maximum value for S_{ice}*of about 1.62 at 210 K, sharply decreasing to about 1.42 at 185 K (see Figure 8b); our new data show instead that S_{ice}* continues to increase with decreasing

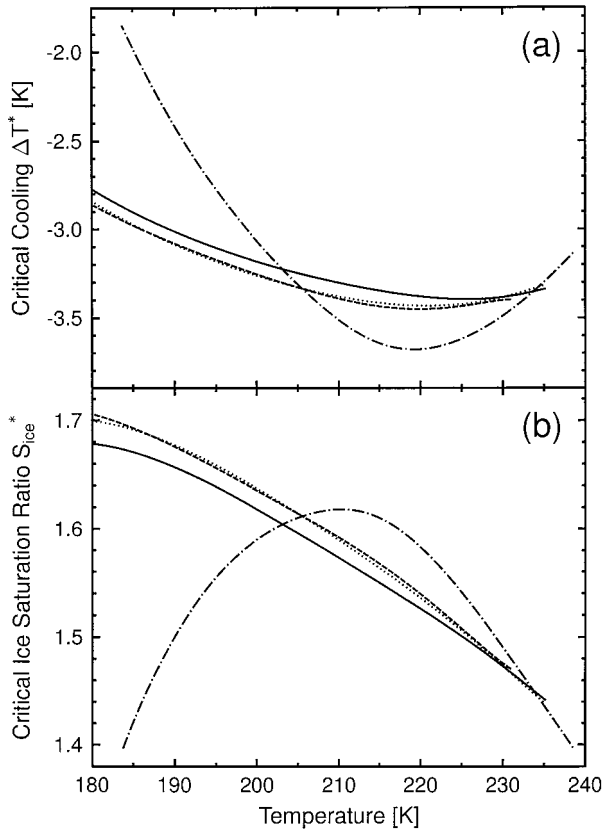

Figure 8. Critical parameters for the nucleation of ice from HNO_3/H_2O and $HNO_3/H_2SO_4/H_2O$ aerosols as a function of temperature: (a) critical cooling below the ice frost point, ΔT*; (b) ice saturation ratio, S_{ice}*. Solid lines: HNO_3/H_2O aerosols. Dotted lines: HNO_3/H_2O aerosols with 1 wt % of H_2SO_4. Dashed lines: HNO_3/H_2O aerosols with 5 wt % of H_2SO_4. Dash−dotted lines: calculations for HNO_3/H_2O aerosols by Tabazadeh et al.[35] Note that the values determined in this work are for aerosols 2.5 μm in diameter, while the calculations by Tabazadeh et al.[35] are for aerosols 0.2 μm in diameter.

temperatures, its values ranging from 1.57 at 210 K to 1.67 at 185 K. This difference is also obvious in the value of the critical supercooling ΔT*, which Tabazadeh et al.[35] estimate to be about −3.5 K at temperatures around 230 K, with a minimum value of about −3.7 at 220 K, rising to approximately −2.0 K at 185 K (see Figure 8a); instead, our new values start at −3.4 K at about 230 K, with only a small increase to −2.9 K at 185 K. This has important consequences for the formation of PSCs.

A comparison of the experimental results with varying H_2SO_4 compositions shows that slightly higher S_{ice}* and ΔT* values are needed for the freezing of ice from ternary aerosols containing 1 and 5 wt % H_2SO_4. However, these differences are within the combined uncertainties of the experimental

freezing point determinations and the water activity model calculations. Thus, the general behavior of increasing S_{ice}* with decreasing temperatures down to ~185 K appears to be independent of the H_2SO_4 content of the HNO_3 solutions. It is interesting to note in this respect that the S_{ice}* and ΔT* values for the three cases with 0, 1, and 5 wt % H_2SO_4 are essentially the same over the entire temperature range while their actual freezing points differ by up to 25 K (see Figure 6).

Table 1 shows the parametrizations for the critical freezing temperature (T_f) as a function of HNO_3 composition and for the critical saturation ratio (S_{ice}*) and the cooling below the ice frost point (ΔT*) as a function of temperature. These parametrizations can be used to calculate the experimental data points directly over the validity ranges given in Table 1. Since the S_{ice}* and ΔT* values agree within experimental error with the results for the binary H_2SO_4 system recently reported by Koop et al.,[32] their parametrizations for S_{ice}* and ΔT* as a function of the atmospheric water partial pressure can be used for atmospheric applications as well.

Previously, it was generally believed that ice would freeze without much supercooling from stratospheric aerosols, and usually, a critical cooling of about 1 K below the ice frost point was assumed.[9] Only recently, Tabazadeh et al.[35] suggested that a value of about 2.0−2.5 K would be more appropriate for binary HNO_3/H_2O at stratospheric temperatures (see Figure 8a). Our new data set suggests a cooling below the ice frost point of about 2.9−3.1 K for both binary HNO_3/H_2O and ternary $HNO_3/H_2SO_4/H_2O$ aerosols containing moderate amounts of H_2SO_4. On the other hand, Carslaw et al.[38] inferred a cooling of 3−4 K from in situ lidar measurements of a stratospheric lee wave ice cloud at 184 K. They stated that a cooling of at least 2.8 K is required to explain the observations. Our experiments suggest that ternary $HNO_3/H_2SO_4/H_2O$ aerosols containing moderate amounts of H_2SO_4 ($\leq$5 wt %) would require a cooling of about 3.0 K below the ice frost point at 184 K.

5. Conclusions

To study the mechanisms of the formation of ice from stratospheric aerosols, we have investigated the liquid−solid phase transitions of emulsified binary HNO_3/H_2O and ternary $HNO_3/H_2SO_4/H_2O$ acid solutions under polar stratospheric conditions using differential scanning calorimetry. Our results indicate that binary solution droplets with less than 33 wt % HNO_3 freeze to form ice at temperatures 37−65 K below the equilibrium melting temperatures, while droplets with higher concentrations (up to 65 wt %) do not freeze but form glasses instead at temperatures below 160 K. The results also show that the presence of H_2SO_4 in amounts corresponding to less than 5 wt % enhances the supercooling below the ice melting point relative to binary HNO_3 droplets by a few degrees Kelvin. A thermodynamic model, incorporating our new freezing temperature data, has been used to predict the formation of solid polar stratospheric clouds. The results indicate that the homogeneous nucleation of ice particles from ternary aerosols requires saturation ratios with respect to ice of greater than about 1.65 at temperatures below 195 K. These saturation ratios correspond to a cooling of about 3 K below the ice frost point, which is in close agreement with recent in situ observations.[38] These ice saturation ratios appear to be independent of the H_2SO_4 or HNO_3 concentration within the ternary $HNO_3/H_2SO_4/H_2O$ system.

Acknowledgment. This work was supported by a grant from the National Science Foundation Atmospheric Chemistry Program. H.-Y. A. Chang thanks the Kann-Rasmussen Foundation for a "Chlorine Project" Fellowship, and T. Koop acknowledges a Feodor Lynen Fellowship from the Humboldt Foundation and an Otto Hahn Fellowship from the Max Planck Society.

References and Notes

(1) Solomon, S. *Nature* **1990**, *347*, 347.

(2) Molina, M. J.; Molina, L. T.; Golden, D. M. *J. Phys. Chem.* **1996**, *100*, 12888.

(3) *WMO Scientific Assessment of Ozone Depletion: 1994*. Global Ozone Research and Monitoring Project, Report No. 37; World Meteorological Organization: Washington, DC, 1995.

(4) Tabazadeh, A.; Turco, R. P.; Drdla, K.; Jacobson, M. Z. *J. Geophys. Res. Lett.* **1994**, *21*, 1619.

(5) MacKenzie, A. R.; Kulmala, M.; Laaksonen, A.; Vesala, T. *J. Geophys. Res.* **1995**, *100*, 11275.

(6) Koop, T.; Carslaw, K. S. *Science* **1996**, *272*, 1638.

(7) Zhang, R.; Leu, M.-T.; Molina, M. J. *Geophys. Res. Lett.* **1996**, *23*, 1669.

(8) Carslaw, K. S.; Luo, B. P.; Clegg, S. L.; Peter, Th.; Brimblecombe, P.; Crutzen, P. J. G*eophys. Res. Lett.* **1994**, *21*, 2479.

(9) Koop, T.; Biermann, U. M.; Raber, W.; Luo, B. P.; Crutzen, P. J.; Peter, Th. *Geophys. Res. Lett.* **1995**, *22*, 917.

(10) Beyer, K. D.; Seago, S. W.; Chang, H. Y.; Molina, M. J. *Geophys. Res. Lett.* **1994**, *21*, 871.

(11) Vonnegut, B. *J. Colloid. Sci.* **1948**, *3*, 563.

(12) Fox, P. G. *Nature* **1959**, *184*, 546.

(13) Broto, F.; Clausse, D. *J. Phys. C: Solid State Phys.* **1976**, *9*, 4251.

(14) MacFarlane, D. R.; Kadlyala, R. K.; Angell, C. A. *J. Chem. Phys.* **1983**, *87*, 235.

(15) Miyazawa, Y.; Pound, G. M. *J. Cryst. Growth* **1974**, *23*, 45.

(16) Perepezko, J. H.; Smith, J. S. *J. Non-Cryst. Solids* **1981**, *44*, 65.

(17) Ji, K. Etudes de la compositions des aerosols stratospheriques polaires au moyen des diagrammes de phase stables, metastables et cinetiques des systems: HNO/H_2O, HCl/H_2O et H_2SO_4/H_2O. Ph.D. Thesis, L'universite de Paris, Paris, 1994 (135 pages).

(18) MacFarlane, D. R.; Angell, C. A. *J. Phys. Chem.* **1982**, *86*, 1927.

(19) Chang, H. Y. A. Experimental Studies of the Formation Mechanisms of Type I Polar Stratospheric Clouds. Ph.D. Thesis, Massachusetts Institute of Technology, Cambridge, MA, 1996.

(20) Menczel, J. D.; Leslie, T. M. *Thermochim. Acta* **1990**, *166*, 309.

(21) Menczel, J. D.; Leslie, T. M. *J. Thermal Anal.* **1993**, *40*, 957.

(22) Borchard, H. J.; Daniels, F. *J. Am. Chem. Soc.* **1957**, *78*, 41.

(23) Borchard, H. J. *J. Inorg. Nucl. Chem.* **1960**, *12*, 252.

(24) Satoh, K.; Kanno, H. *Bull. Chem. Soc. Jpn.* **1982**, *55*, 1645.

(25) Hallett, J.; Lewis, R. E. S. *Weather* **1967**, *22*, 56.

(26) Uhlmann, D. R. In *Kinetics of Reactions in Ionic Systems*; Gray, T. J., Frechette, V. D., Eds.; Plenum Press: New York, 1969.

(27) Disselkamp, R. S.; Anthony, S. E.; Prenni, A. J.; Onasch, T. B.; Tolbert, M. A. *J. Phys. Chem.* **1996**, *100*, 9127.

(28) Tsias, A.; Prenni, A. J.; Carslaw, K. S.; Onasch, T. P.; Luo, B. P.; Tolbert, M. A.; Peter, T. *Geophys. Res. Lett.* **1997**, *24*, 2303.

(29) Prenni, A. J.; Onasch, T. B.; Tisdale, R. T.; Siefert, R. L.; Tolbert, M. A. *J. Geophys. Res.* **1998**, *103*, 28439.

(30) Bertram, A. K.; Sloan, J. J. *J. Geophys. Res.* **1998,** *103*, 3553.

(31) Bertram, A. K.; Sloan, J. J. *J. Geophys. Res.* **1998**, *103*, 13261.

(32) Koop, T.; Ng, H. P.; Molina, L. T.; Molina, M. J. *J. Phys. Chem.* **1998,** *102*, 8924.

(33) Koop, T.; Luo, B. P.; Biermann, U. M.; Crutzen, P. J.; Peter, T. *J. Phys. Chem. A* **1997**, *101*, 1117.

(34) Meilinger, S. K.; Koop, T.; Luo, B. P.; Huthwelker, T.; Carslaw, K. S.; Krieger, U.; Crutzen, P. J.; Peter, T. *Geophys. Res. Lett.* **1995**, *22*, 3031.

(35) Tabazadeh, A.; Toon, O. B.; Jensen, E. J. *Geophys. Res. Lett.* **1997**, *24*, 2007.

(36) Tabazadeh, A.; Jensen, E. J.; Toon, O. B. *J. Geophys. Res.* **1997**, *102*, 23845.

(37) Carslaw, K. S.; Clegg, S. L.; Brimblecombe, P. *J. Phys. Chem.* **1995**, *99*, 11557.

(38) Carslaw, K. S.; Wirth, M.; Tsias, A.; Luo, B. P.; Dörnbrack, A.; Leutbecher, M.; Volkert, H.; Renger, W.; Bacmeister, J. T.; Peter, T. *J. Geophys. Res* **1998**, *103*, 5785.